Ce AND Fe COMPLEXES AS POTENT ANTIFUNGAL AGENTS FOR WALLPAPERS

Rania H. Taha[1,2*], Nowarah J Almutlq[2], Tarek A. Seaf Elnasr[2,3], Mutairah S. Alshammari[2],
Sabrein H. Mohamed[2,4] and Shaimaa M.N. Moustafa[5]

[1]Department of Chemistry, Faculty of Science (Girls), Al-Azhar University, P.O. Box: 11754,
Yousef Abbas Str., Nasr City, Cairo, Egypt
[2]Chemistry Department, College of Science, Jouf University, P.O. Box: 2014, Sakaka,
Saudi Arabia
[3]Department of Chemistry, Faculty of Science, Al-Azhar University, Assiut, Egypt
[4]Chemistry Department, Faculty of Science, Cairo University, Giza, Egypt
[5]Biology Department, College of Science, Jouf University, Sakaka, Saudi Arabia

ABSTRACT. The current research focused on the Schiff base ligand (S,E)-2-((2-hydroxy-3-methoxy-benzylidene)amino)-3-(1H-imidazol-4-yl)propanoic acid which synthesis by reacting L-histidine and 2-hydroxy-3-methoxy-benzaldehyde. Its complexes with Ce(III) and Fe(III) both in bulk and nano size were also synthesized. The ligand and its metal complexes were characterized by various physicochemical methods such as FT-IR, ^{1}H NMR, ^{13}C NMR, electronic spectra, XRD, TGA, and SEM. The synthesized ligand and its metal complexes were screened against different fungi. It was found from the results that the cerium nano complex shows a potent antifungal activity for indoor uses as wallpapers.

KEY WORDS: Schiff base ligands, Nano complexes, Ce nano complexes, Wallpapers

INTRODUCTION

Due to the interior environment's high moisture content, fungus, among other dangerous microbes, is the most common occupant that may grow on wallpaper (paper glued on building walls) [1].

Aspergillus, *Fusarium*, *Cladosporium*, *Penicillium*, *Paecilomyces*, and *Acremonium* are the most often occurring species implicated in the colonization of the wall, which may result in allergies or infection. These fungi can produce mycotoxins, which can enter the body through skin contact or inhalation and cause a variety of reactions and symptoms [2]. Every species of fungus does indeed have a distinctive set of antigenic and allergic components that can cause coughing, wheezing, sore eyes and throats, skin infections, diarrhea, nasal congestion, headaches, and nausea, as well as a higher chance of developing asthma [3, 4]. An important aspect of nanotechnology is the advancement of green nanoparticle production. Due to their practicality and lack of pollution, green-derived nanoparticles are becoming increasingly popular [5, 6]. Physical, chemical, and biological processes can all produce nanoparticles. The most common techniques for creating nanoparticles are chemical ones. The production of silver nanoparticles is a quick, easy, environmentally safe, and economically viable process. The size and shape of the nanoparticles affect the silver's stability [7]. Silver is still the best metal for the formation of nanoparticles due to its broad antibacterial and antifungal actions, as well as its ability to interact with a wide range of ligands and proteins in microbial cells [8]. Currently available antifungal agent for indoor usage must be non-volatile, odorless, hypoallergenic, and non-toxic to humans and other animals [9]. To prevent the growth of microorganisms on construction materials, the proper biocides must be used [10]. As a result, in this study, nanoparticles were created utilizing several methods to create environmentally friendly antifungal biocide that was affordable, quick, easy to acquire, and

_____

extremely effective. The isolated fungus from the polluted wall were recognized by microscopic inspection [11, 12].

The chemistry of Schiff bases, which are the most versatile starting chemicals in coordination chemistry, has been intensively researched during the past decades. With potent antimicrobial, antiviral, anticancer, and antioxidant characteristics, Schiff bases find widespread use in the biological sciences [13].

The excessive use of antimicrobials has considerably contributed to the growth of drug-resistant bacteria, which remain a top cause of death globally. Infectious germs are a major threat to humanity because there are now no effective cures. Antimicrobial resistance is an increasing problem, thus researchers are creating new classes of antimicrobial medications with effective ways to counteract it. Recently, transition metal complexes have become increasingly common [14]. The main objective of this study is to prepare different compounds and elucidate their structures by different physicochemical and spectral methods then investigate their activities as potent antifungal agents to be used as wallpapers.

EXPERIMENTAL

L-Histidine, 2-hydroxy-3-methoxy-benzaldehyde, $Fe(NO_3)_3.6H_2O$, $Ce(NO_3)3.6H_2O$, and C_2H_6O, among other things, were acquired from (Aldrich) and used without further purification.

On a 600 MHz spectrometer, the ^{13}C and ^1H NMR spectra (in DMSO-*d6*) were obtained without the use of an internal standard. In the central laboratory of Jouf University, thermal analyses were conducted utilizing a thermogravimetric analyzer in a dynamic nitrogen environment with 10 °C/min rate of heating. Molar conductance was determined at room temperature utilizing a JEN WAY 4510 conductivity meter and C_3H_7NO (DMF) as a solvent.

Employing a Perkin-Elmer 437 IR spectrometer, the IR spectra were measured as KBr discs (400-4000 cm^{-1}). Thermogravimetric analyzers DTA, TA50 Shimadzu and TGA-50 SHIMA VZU were used to conduct thermal analyses in dynamic nitrogen atmosphere with 10 °C min^{-1} heating rate.

Synthesis of the free ligand

The ligand was produced utilizing procedures that had previously been published [15]. An ethanolic solution of 2-hydroxy-3-methoxy-benzaldehyde (3.05 g, 0.025 mol) was included to an ethanolic solution of L-histidine (3.88 g, 0.025 mol) and the reaction combination was refluxed for 2 hours in a water bath. Filtration was used to collect the product, which was then cleaned multiple periods with $C_2H_5OC_2H_5$ and ethanol before being dehydrated in a desiccator over anhydrous $CaCl_2$ to provide a dark yellow powder with a 97% yield.

Fe metal complex's synthesis in bulk size

An ethanolic solution of metal ions $Fe(NO_3)_3.6H_2O$, (0.01 mol) was added separately dropwise with continual stirring to an ethanolic solution of the ligand (0.01 mol) (1:1 molar ratio). After that, the subsequent solutions were then refluxed for 3 h whereupon a change of color followed by the formation of precipitates was observed. The precipitated complex was filtered off, rinsed for numerous periods with $C_2H_5OC_2H_5$ and ethanol then dehydrated in a desiccator over anhydrous $CaCl_2$ [16]. The powder of the compound is constant in air, dissolved in DMSO and DMF, but insoluble in the majority of organic solvents.

Synthesis of Ce nano metal complex

To generate nano-scale complex, a solution of the ligand (0.1 mmol) in 10 mL of $CHCl_3/CH_3OH$ 2:1 (V: V) was combined with a solution of $Ce(NO_3)_3.6H_2O$ (0.1 mmol) in 10 mL of CH_3OH. The solution was loaded into an autoclave lined with Teflon and heated at 450 °C for 24 hours before being cooled to room temperature. The product underwent filtration, drying, and characterization [17].

Isolation of fungal species

One cm square piece of different wallpapers were placed in a flask with 5 mL of sterilized H_2O and shaken well. Then 1 mL of suspension was pipette into Petri plates, and PDA pour-plates were prepared. The inoculated Petri dishes were then incubated at 26 ºC for 6 days and examined. Fungal colonies appeared and were purified for identification.

Identification of fungal isolates

The pure cultures of isolated fungi were identified based on morphological characteristics with the help of identification keys [18, 19].

Determination of the minimum inhibition concentration and minimum fungicidal concentration

Broth microdilution protocols were used to determine the minimum inhibitory concentration (MIC) of Microbial cultures with some modifications. The 100 µL of the dilution series (0.005, 0.01, 0.02, 0.04, 0.05, 0.1, 0.2, 0.3, 0.4 and 0.5 mg/mL) were performed on a 96-well-microplate containing growth media (PDB). After adding 30 µL of spore suspension (10^7 CFU/mL), seven days were spent incubating plates at 28.2 °C with positive controls (miconazole). The concentration of an antimicrobial that will completely halt the growth of a microorganism is called its minimal inhibitory concentration (MIC). 48 hours of incubation should be enough to see some growth [20].

Antimicrobial potency testing: identifying the most effective substance

The antimicrobial activity of the tested materials (0.05 mg/mL) was evaluated by the agar-well diffusion method. One ml of each spore suspension (10^7 CFU/mL) was placed in petri dishes (9 cm) that had 15 mL of sterilized PDA media. After solidification, the wells (0.5-mm-diameter) were formed by using a cork borer. The well was filled with 100 µL of tested compounds (H_2L) and its metal complexes (**1**, **2**). The petri dishes were then incubated at 30 °C. The antifungal activity of the samples was measured by determining the diameter of the inhibition zone. All the experiments were repeated three times.

Coatings bio-resistance test

Preparation of treated wallpaper

Sterilized wall paper was cut into samples of 50 mm x 50 mm, and an equal volume (100 mL) of a 3% solution of carboxymethylcellulose (CMC) and complex (**2**) was mixed. The sterilized wall papers were then sprayed and coated. After the preparation, the wall paper was spread in the sterile, opened Petri dish and allowed to dry overnight at room temperature.

Study the evolution activity of treated wall paper during different period

The antifungal activities of the complex (**2**) against isolated fungi were tested by the number of colonies method. The fungus suspension was prepared by inoculating of each isolated fungal

separately in 50 mL of Potato Dextrose Broth (PDB) media. Then the system was shaken for 12 h at 37 °C. The actual number of cells used for a given experiment was determined by the standard serial dilution method. Fungal suspensions (0.05 mL) and 24.5 mL new PDB media were placed into a centrifuge tube to prepare the fungal suspension. All sample of wall paper were sterilized by autoclaving, and then placed under UV light to sterilize for 1 h. The treated wall paper samples (25 mm×25 mm) were put into the fungal suspension (1×10^7 CFU/mL), and then were incubated for 24 h, at room-temperature. The wall paper were get back from cultures and washed by saline solution. The washing solutions were collected and diluted with deionized water until the dilution concentration becomes 10^{-3} of the original value. 50 μL of dilution solution was spread onto PDA culture medium, all plates were incubated for 4 days at 27 °C. The numbers of colonies on the petri dishes were determined by counting method.

The fungistasis rate (F R) of wall paper was calculated by the following equations.

$$\frac{Nc-Nt}{Nc} \times 100 \tag{1}$$

where Nc is the number of colonies on plate (control) and Nt is the number of colonies on the plates that treated with the coated wall paper.

Statistical the analysis

The experimental data were statistically investigated using ANOVA and one-tailed unpaired Student's t-test for significance testing, where $p < 0.05$ was considered significant. Values are presented as the mean ± SD of the three replications in each experiment.

RESULTS AND DISCUSSION

(E)-N-(4,6-dimethylpyrimidin-2-yl)-4-(((2-hydroxynaphthalen-1-yl)methylene)amino)   benzene sulfonamide ligand and its nano metal

Interaction of L-histidine with 2-hydroxy-3-methoxy-benzaldehyde in a one-step condensation reaction readily gives rise to a new imine ligand, H_2L which was used as a compound for further syntheses of metal complexes. This ligand has numerous potential donor sites; imine group (C=N), carboxylic group (COOH), and hydroxyl group (OH). As its structure demonstrates, this ligand can function as a multidentate ligand.

Molar conductivity estimations

The metal compounds were dispersed in DMF, and the 10^{-3} M solutions' molar conductivities were determined at 25 °C. The data shows that the metal complexes' molar conductance values, and the results demonstrate that the metal complexes have molar conductance values of 64.3 and 169.8 $ohm^{-1}mol^{-1}cm^2$ for complexes (**1**) and (**2**), consecutively, implying that these complexes are 1:1 and 1:3 electrolytic in nature and verifying the existence of ionic nitrate anions in complexes. All metal complexes' molar conductivities were calculated at 25 °C in a DMF solvent with a level of 1.0×10^{-3} M. [12, 22, 23].

Infrared spectra investigation

A comparison between the free ligand's IR spectrum, H_2L, and the spectra of its metal complexes shows the binding sites in the ligand that are accessible for coordination with the metal ions. The lack of a band attributed to amino group of L-histidine as well as appearance of one band corresponding to hydroxyl group of 2-hydroxy-3-methoxy-benzaldehyde at 3490 cm^{-1} indicating Schiff base condensation in 1:1 molar ratio [24]. Presence of the new strong band at 1550 cm^{-1}

allocated to imine group [25] as the main characteristic band support generation of the suggested structure of the ligand. At 3490 cm^{-1}, the IR ligand spectra reveals a large absorption band related to the phenolic and carboxylic groups [26]. The IR spectrum exhibits also clear and medium bands at 1628 and 742 cm^{-1} may be allocated to $\upsilon_{C=O}$ and υ_{C-OH} of carboxylic group, as well as a band at 1217 owing to υ_{C-O} (phenolic group) [26].

In addition, the band at 3490 cm^{-1} is moved to a lower frequency area at 3150-3100 cm^{-1} in all metal complexes, indicating the participation of OH groups of carboxylic and phenolic groups in establishment of complexes without their deprotonation. The spectra of all metal complexes demonstrate the lack of the band at 1628 cm^{-1} supplemented with presence of two characteristic bands at 1625-1616 cm^{-1} and 1394-1318 cm^{-1} related to υ_{asym} (COO$^-$) and υ_{sym} (COO$^-$) consecutively demonstrating the carboxylate oxygen atom's participation in coordination, furthermore, the difference between the symmetric and asymmetric stretching frequencies of the coordinated carboxyl group lies in the range 298-231 cm^{-1}, indicating the monodentate coordinating mode of the COOH group. The strong bands at 1550 and 1217 cm^{-1} owing to $\upsilon_{C=N}$ and υ_{C-O} (azomethine and phenolic groups) are moved to lower or higher wave number (1541-1500 cm^{-1}) and (1221-1220 cm^{-1}), consecutively in all metal compounds revealing the azomethine nitrogen and phenolic oxygen to the metal ions' coordination.

All complexes' IR spectra exhibit strong bands at 1320 cm^{-1} characteristic to υ_{NO3^-} (ionic) modes. In addition to 3 bands at 1410-1400 cm^{-1}, 1395-1390 cm^{-1} and 1150-1100 cm^{-1} comparable to nitrate group's unidentate coordination mode. Conclusive proof of the bonding is also demonstrated by noticing novel bands in the metal complexes' IR spectra in low frequency region at 536-500 cm^{-1} and 457-420 cm^{-1} may be owing to υ_{M-O} and υ_{M-N}, consecutively [23]. Furthermore, it is problematic to illustrate conclusions dependent on υ_{OH} to reveal the water molecules' nature owing to the various likelihoods in the υ_{OH} water area culminated from the existence of υ_{OH} of the carboxylic and phenolic groups as well as water molecules connected with the compound configuration. Using the thermal gravimetric analysis method, the nature of H$_2$O molecules was recognized as completely clear.

^{1}H NMR spectra investigation

The free ligand, H$_2$L and its metal complexes' ^{1}H NMR spectra, were measured in DMSO-d6 at room temperature. The chemical shifts were distinguished in portions per million (ppm). In the free ligand, H$_2$L^2 spectrum, the singlet signals at δ 11.32, 8.56, 8.41 and 8.23 ppm were attributed to carboxylic, phenolic or NH and azomethine protons, respectively, while the multiplet that appeared at δ 6.70-7.59 ppm is associated with aromatic protons [27, 28]. Comparing the ^{1}H NMR data of the free ligand and its complexes explains the coordination method among the ligand and its metal ions. Upon complexation, it was established that the metal complexes' spectra exhibit a significant change of the signals because of phenolic, azomethine, and carboxylic protons, revealing the azomethine group's participation in coordination as well as both carboxylic and phenolic groups' participation in organization to the metal ions deprived of their deprotonation, asserting that the ligand behaves as a neutral tridentate ligand, ONO coordination sphere.

Thermal gravimetric studies (TGA)

The thermal decomposition of the new synthesized ligand exhibits two consecutive decomposition steps Table 1. The initial step at a temperature scale 200-340 °C with a mass loss of 29.165% (calcd. 31.111%) corresponded to the removal of one mole of NO, N$_2$ and O$_2$ gases. The second decomposition step with a temperature range of 340–600 °C with a mass loss of 32.72% (calcd. 31.522 %) corresponded to the elimination of C$_5$H$_{15}$O. The overall mass loss amounting to 61.885% (calcd. 62.633%) leaving nine carbon atoms as a final residue.

The thermal decomposition of $[Fe(H_2L)(NO_3)_2(H_2O)]NO_3 \cdot H_2O$ complex displayed three decomposition steps. The initial step at a temperature range 40-313 °C with a mass loss of 25.357% (calcd. 25.045%) corresponded to the exclusion of one molecule of water (hydrated), one water molecule (coordinated), and one mole of each NO_2, N_2 and O_2 gases. The second decomposition step with a temperature range of 331-400 °C involved a 17.224% mass loss due to elimination of $C_5H_{10}NO$ (calcd. 17.657%). The third decomposition step (400-600 °C) resulted in releasing of $C_2H_5N_2O_6$ and ½ O gas with a mass loss of 28.688 % (calcd. 28.398%) leaving ½ Fe_2O_3 and seven carbon atoms as a final residue with overall mass loss amounting to 71.269% (calcd. 71.1 %).

The thermal decomposition of $[Ce(H_2L^2)(H_2O)_3] \cdot 3NO_3$ nano-complex (**5**) displayed three decomposition steps. The initial step is at a temperature scale 40-210 °C with a mass loss of 21.12% (calcd. 21.51%) corresponded to the removal of three molecules of coordinated water and NO_2, N_2, ½O_2. The second decomposition step with a temperature scale of 210-410 °C involved a 50.30% mass loss due to elimination of $C_{10}H_{15}N_3O_{10}$ (calcd. 51.26%). The third decomposition step (410-600 °C) resulted in releasing of 4C with a mass loss of 7.11% (calcd. 7.17%) leaving Ce metal as a final metallic residue with overall mass loss amounting to 78.53% (calcd. 79.94%).

Table 1. Synthesized ligand, H_2L and its metal complexes' thermogravimetric data.

Ligand/Complex	Stage	Temp. range (°C)	Mass loss (%)		Evolved moiety	Residue moiety
			Found	Calcd.		
H₂L	I	200-340	29.165	31.111	NO, N_2, O_2	$C_{14}H_{15}O$
	II	340-600	32.72	31.522	$C_5H_{15}O$	9C
(1)	I	40-313	25.357	25.045	H_2O lattice, H_2O Coord., NO_2, N_2, O_2	$C_{14}H_{15}N_3O_9Fe$
	II	331-400	17.224	17.657	$C_5H_{10}NO$	$C_9H_5N_2O_8Fe$
	III	400-600	28.688	28.398	$C_2H_5N_2O_6$, ½ O	½ Fe_2O_3, 7C
(2)	I	40-210	21.12	21.51	3H_2O Coord., NO_2, N_2, ½O_2	$C_{14}H_{15}N_3O_{10}Ce$
	II	210-410	50.30	51.26	$C_{10}H_{15}N_3O_{10}$	C_4Ce
	III	410-600	7.11	7.17	4C	Ce as a metallic residue

Electronic absorption spectral studies

The electronic absorption spectra of the ligand and its metal complexes (**1**, **2**) in DMF solution were carried out in the range of 200-800 nm at room temperature. There is a shift of the bands to longer λ in spectra of all metal complexes which is a good evidence of complex formation. The bands observed at 268 nm and 278, 280, 285 nm for the ligand and its metal complexes are attributed to intraligand π-π* transition of phenyl group. Band between 320 nm in case of the ligand is due to n-π* transition. It is inferred from the electronic transitions that the azomethine group present in the ligand.

Fe(III) complex (**1**) has one absorption band at 580-589 nm due to the transition $^6A_{1g} \rightarrow T_{2G}$ in octahedral geometry [29].

In UV spectrum of the cerium complex (**2**), there is no noticeable absorption in the visible region (380 nm to 700 nm) due to the shielding effect of rare earth 4f orbital electron (Figure 1) [30].

Powder X-ray diffraction analysis

The X-ray diffraction (XRD) patterns of complexes (**1**, **2**) and their parent ligand, **H₂L**, were performed at room temperature within the range of 5 < 2θ < 80°. Comparing the XRD patterns of

all of the investigated substances, Figure 2. In addition to the formation of new peaks at various 2θ and d-spacing values, there are notable differences in the position and relative strength of some peaks at position. Such a transformation may be attributable to the production of new phases as a result of the bonding of metal ions and the formation of metal complexes, in which the metal complexes have a distinct structure that is not contaminated by the ligand, **H₂L**. All data related with the acquired diffractograms, including 2θ values for each peak, relative intensity, and interplanar spacing (d-values), are compiled and summarized in Table 2.
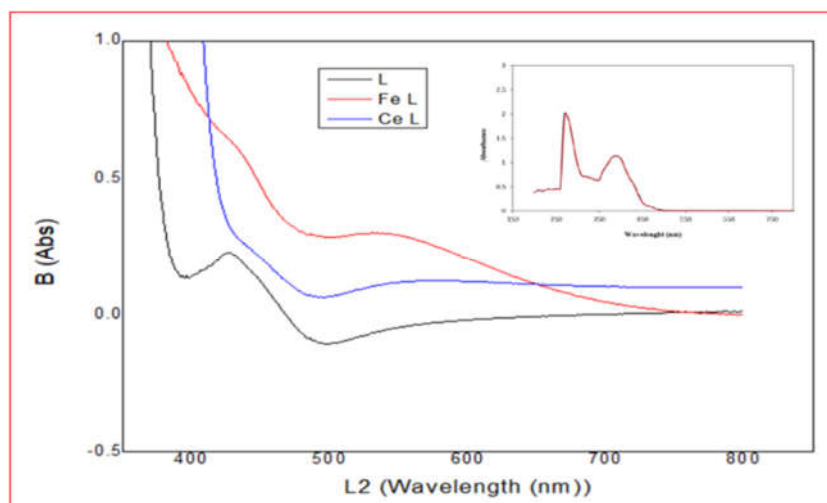

Figure 1. UV-Vis spectra of the ligand H₂L and its metal complexes.

In addition, X-ray diffraction is a useful technique for estimating the average size of nanocrystalline and bulk materials [31]. In 1981, the first scientist, Paul Scherrer, reported his findings in a publication that included the Scherrer equation [32]. This is due to the fact that "crystallite size" and "particle size" are not synonymous, yet X-Ray diffraction is sensitive to the crystallite size within the particles. D, the size of crystallites, can be estimated using Scherrer's formula, equation 2:

$$D = \frac{K\lambda}{\beta \cos\theta} \tag{2}$$

where: λ: the X-ray wavelength in nanometers, β: is the width of the diffraction peak caused by small crystallite size (FWHM) in radians, K: Scherer constant typically has a value of 0.9 when crystallite shape is considered, and θ: peak position in radians.

The results of applying the above equation to the obtained X-ray data indicate that the grain size is 14,99, 16,30, and 2.01 nm for the prepared ligand and its metal complexes (**1**, **2**), respectively, and that complex (**2**) has the smallest grain size compared to the parent ligand and all other prepared compounds (Tables 3, 3 continuous).

Micromorphology of the prepared compounds

Using scanning electron microscopy (SEM), the ligand and its metal complexes' micromorphology was studied; the results are depicted in Figure 3. It was noted that all components were homogeneous and densely distributed, with diameters ranging from 150 to 200

μm. It revealed that the ligand's size, around 12 μm, was more than the size of the metal complexes. Its metal complexes have a diverse (0.12 μm) and sparse microsphere size distribution.

As a result of the metal ions' coordination with the ligand's donor sites, the ligand's micrographs and its metal complexes differ dramatically. Moreover, SEM micrographs of metal complexes indicated that the type of the metal ion affects the metal complexes' surface shape [33].

Particle size distribution

The ligand and its metal complexes' particle size distribution was determined, and the findings are displayed in (Figures 4a-c). The particle size distribution of the complexes was observed to be narrow, mostly spread between 100 and 400 μm, with the bulk concentrated at 200 μm, which was similar with the SEM observation.

Table 2. Calculation of grain size for the synthesized ligand **H₂L**.

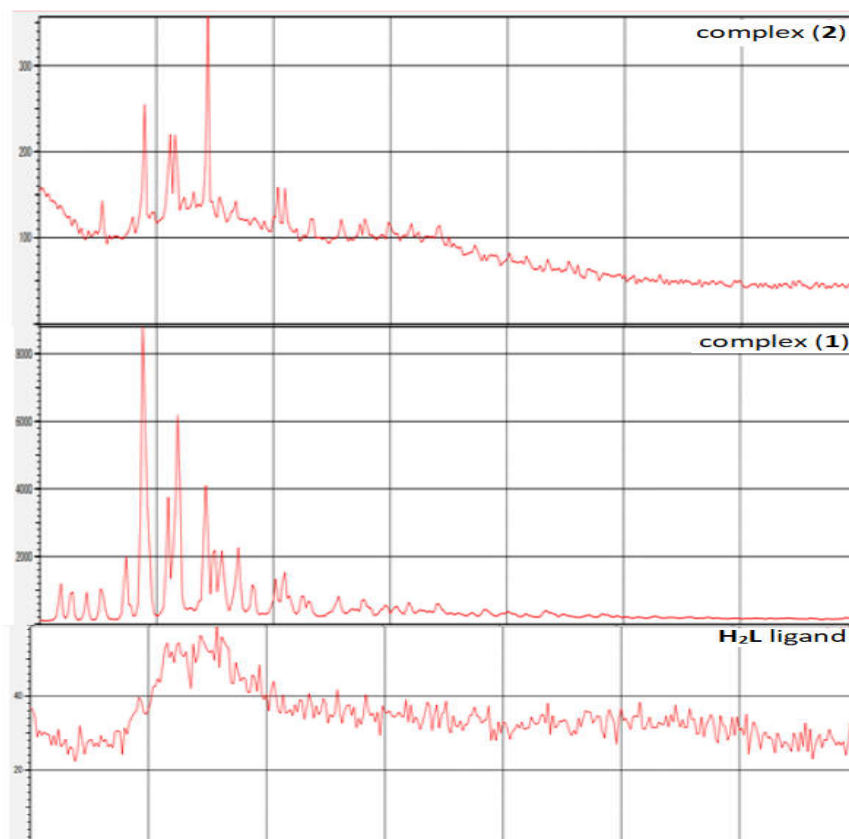| Peak position (2Theta), deg	Theta, Radians	FWHM, deg	FWHM, Radians	Crystallite size (D), nm
11.9743	0.10450	0.57500	0.0100	13.89193
15.4216	0.13458	0.45330	0.0079	17.68537
17.8684	0.15593	0.36800	0.0064	21.85288
19.0168	0.16595	0.53900	0.0094	14.94425
21.2593	0.18552	0.73100	0.0128	11.05745
21.6583	0.18900	0.69720	0.0122	11.60116
24.3996	0.21293	0.50350	0.0088	16.14269
25.6499	0.22384	0.56360	0.0098	14.45626
26.7147	0.23313	0.91110	0.0159	8.961884
28.4454	0.24823	0.71420	0.0125	11.47507
29.2443	0.25520	0.43340	0.0076	18.94371
30.2430	0.26392	0.39100	0.0068	21.04662
31.0420	0.27089	0.52180	0.0091	15.801
33.3014	0.29061	0.49720	0.0087	16.67735
35.8508	0.31286	0.52740	0.0092	15.83162
37.2360	0.32495	0.33340	0.0058	25.14393
37.8355	0.33018	0.77040	0.0134	10.9007
39.2344	0.34238	0.68580	0.0120	12.29778
40.0338	0.34936	0.87280	0.0152	9.687264
41.8609	0.36531	1.35670	0.0237	6.269277
44.2312	0.38599	0.54540	0.0095	15.72277
45.8303	0.39994	0.53340	0.0093	16.16976
47.2153	0.41203	0.54280	0.0095	15.97251
48.7788	0.42568	0.70000	0.0122	12.461
50.1582	0.43771	0.46000	0.0080	19.06784
51.6428	0.45067	0.51060	0.0089	17.28448
53.4560	0.46649	0.36990	0.0065	24.04615
55.2483	0.48213	0.54470	0.0095	16.46114
55.9258	0.48804	0.40000	0.0070	22.48592
57.0254	0.49764	0.48580	0.0085	18.61021
57.4252	0.50113	0.28000	0.0049	32.35023
				Average=16.30

Figure 2. X-ray diffraction data of **H₂L** ligand, (**1**) and (**2**) complexes.

Table 3. Calculation of grain size for the complex **1**.

Peak position (2Theta), deg	Theta, Radians	FWHM, deg	FWHM, Radians	Crystallite size (D), nm
11.6883	0.10200	0.30660	0.0054	26.0463
12.7695	0.11143	0.55360	0.0097	14.4398
14.0455	0.12257	0.48870	0.0085	16.37884
15.3698	0.13413	0.57480	0.0100	13.94622
17.4246	0.15206	0.54580	0.0095	14.72522
18.9527	0.16539	0.64880	0.0113	12.41399
20.8604	0.18204	0.29120	0.0051	27.73958
21.8270	0.19048	0.63810	0.0111	12.67923
24.2654	0.21176	0.63650	0.0111	12.76636
25.6499	0.22384	0.57840	0.0101	14.08635
26.9821	0.23546	0.62520	0.0109	13.06737
28.2842	0.24683	0.55870	0.0098	14.66365
30.0433	0.26218	0.36760	0.0064	22.37586
31.0420	0.27089	0.71400	0.0125	11.54757
32.6402	0.28484	0.78680	0.0137	10.52088
33.2396	0.29007	0.35180	0.0061	23.56635

35.5452	0.31019	0.72470	0.0126	11.51156
37.8246	0.33008	0.86650	0.0151	9.691435
39.5838	0.34543	0.77880	0.0136	10.84108
40.5026	0.35345	0.80630	0.0141	10.50197
41.6621	0.36357	0.57150	0.0100	14.87297
44.1532	0.38531	0.74700	0.0130	11.47635
				Average = 14.99

Table 3 continuous…..

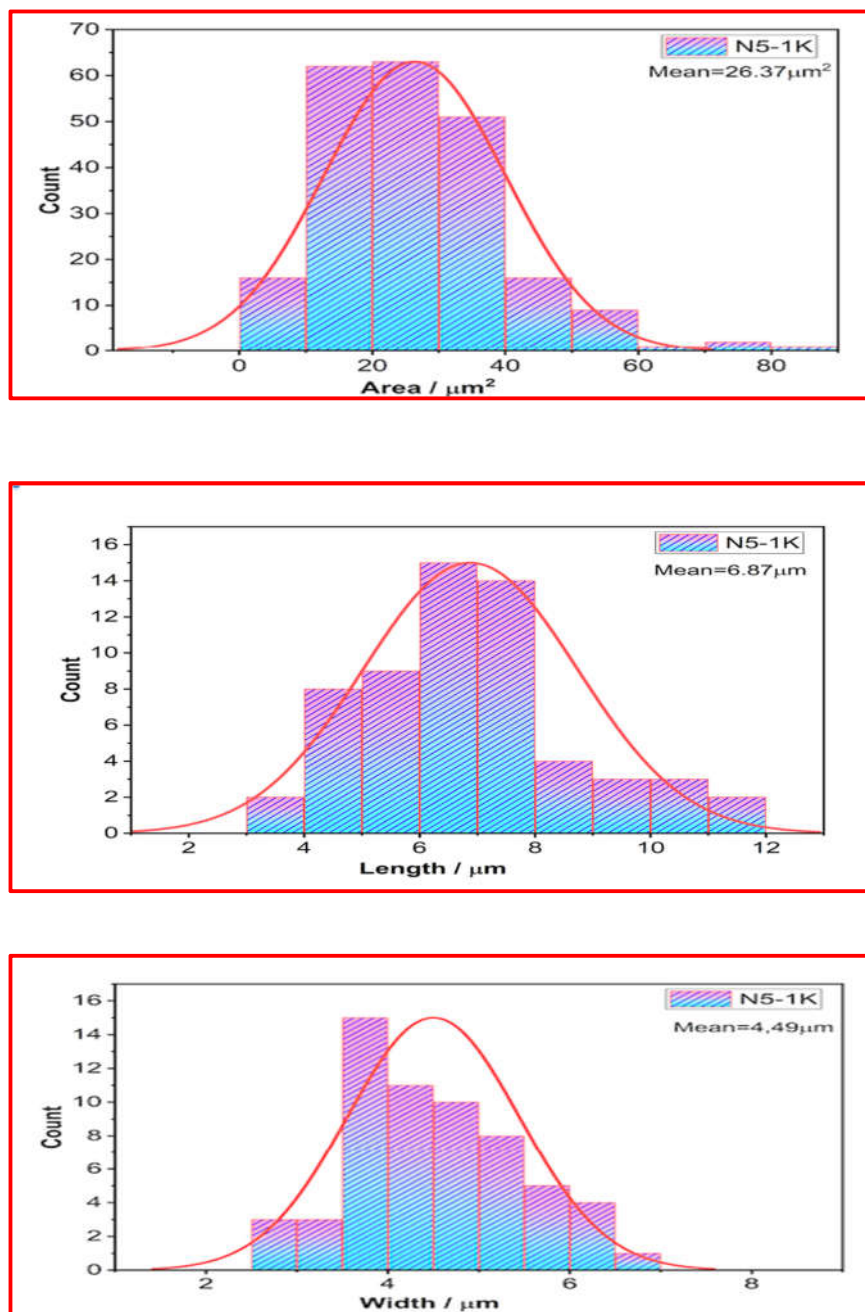| Peak position (2Theta), deg	Theta, Radians	FWHM, deg	FWHM, Radians	Crystallite size (D), nm
24.8180	0.21658	8.46670	0.1478	0.960743
42.8320	0.37378	2.00000	0.0349	4.266747
62.0237	0.54126	11.60000	0.2025	0.799071
				Average = 2.01
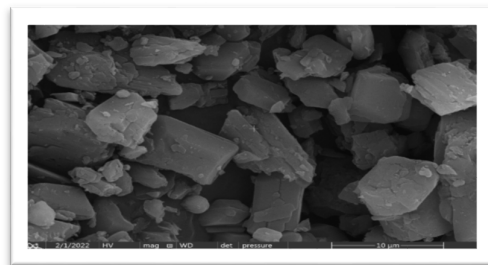
(a)
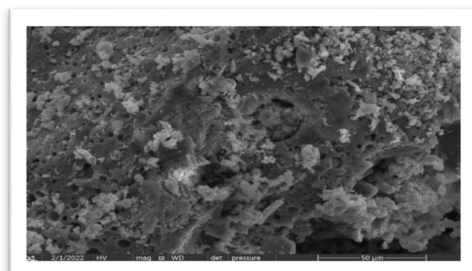
(b) Fe
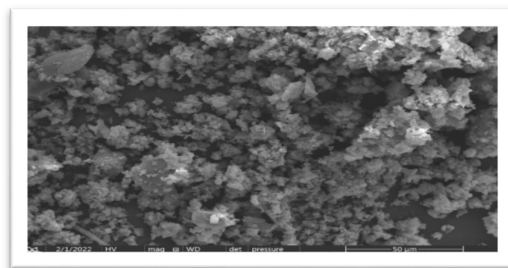
(c) Ce

Figure 3. SEM photograph of the ligand and its metal complex.

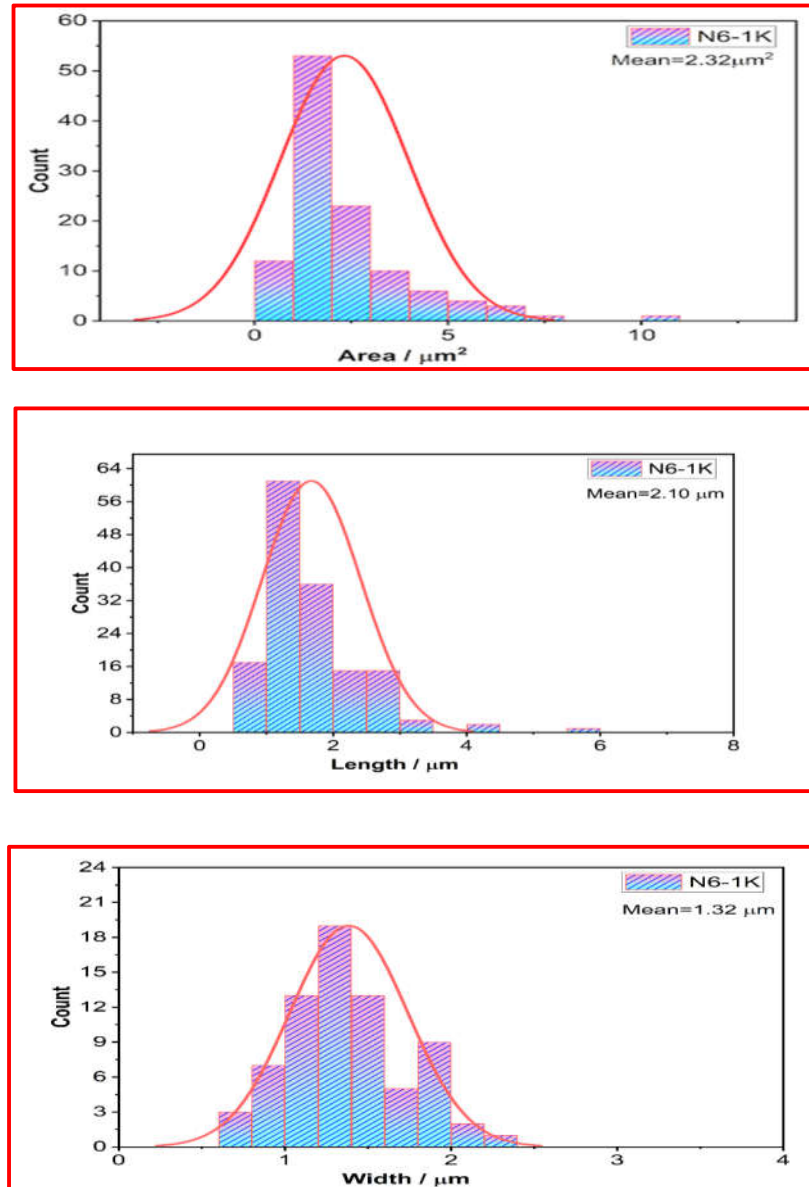Figure 4a. Histogram of the partical distrbation of the **H₂L** ligand.

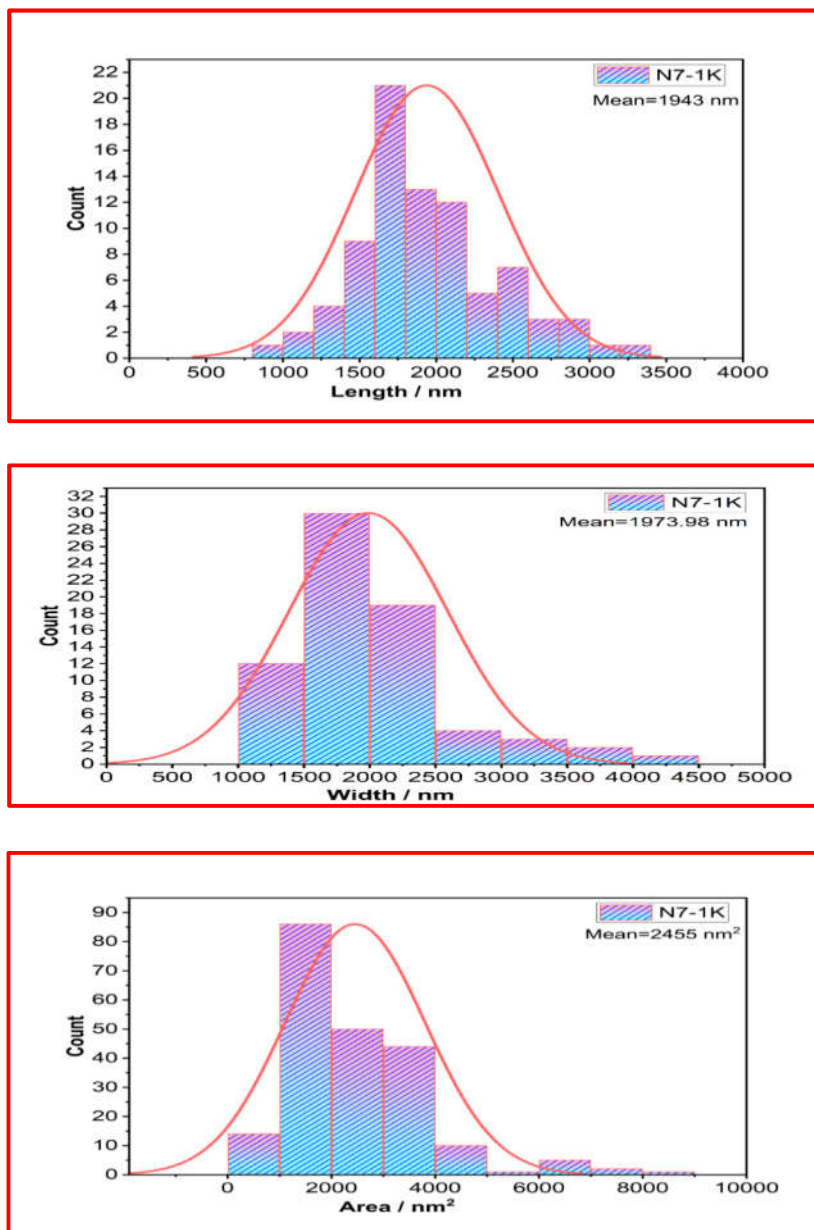Figure 4b. Histogram of the partical distrbation of the complex (**1**).

Figure 4c. Histogram of the partical distrbation of the complex (**2**).

Based on the correlation of all these data, the expected structure for the ligand and its metal complexes are as in Figure 5.
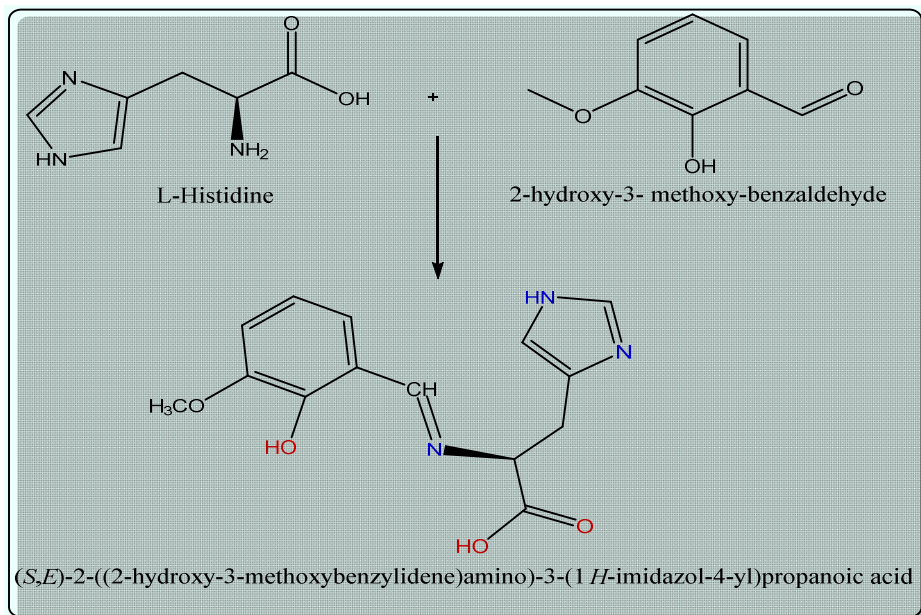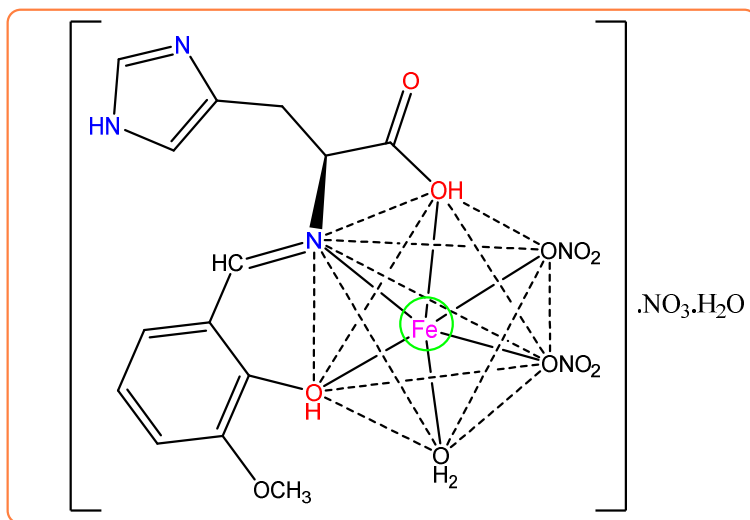

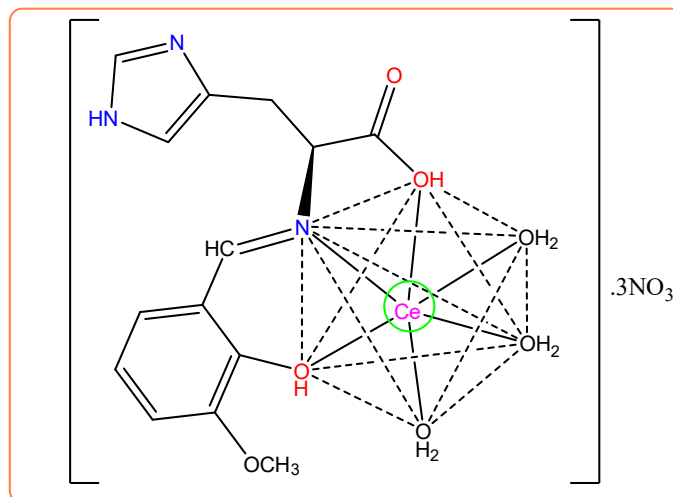Figure 5a. Schematic representation of the tridentate ligand H_2L.

Figure 5b. Suggested structure of the metal complexes **(1, 2)**.

Identification and isolation of fungi

The study was started by isolating and identification of important fungi from wall paper which are one of the dangerous diseases to humans. It was found that as shown in Figure 6a, 6 species belonging to 6 genera were isolated from 5 samples.
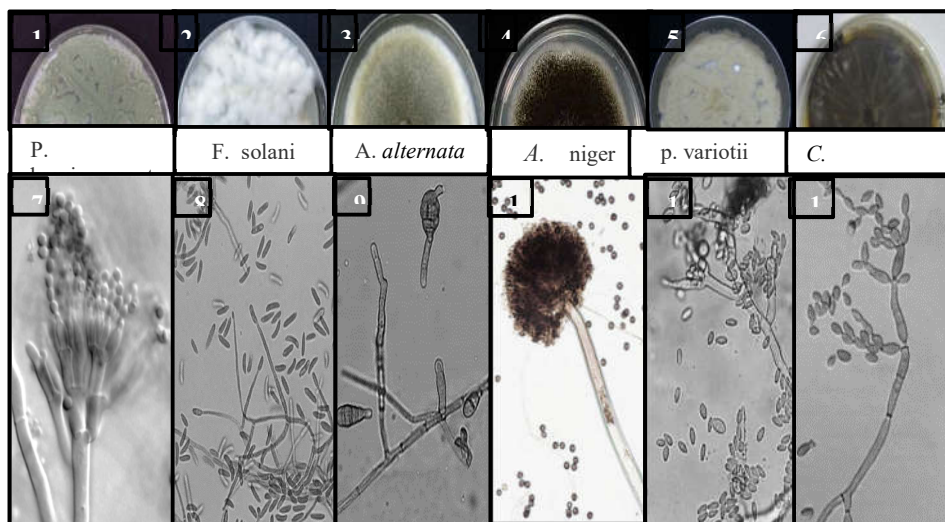

Figure 6a. (1-6) Mycelial growth of isolated fungi on PDA at 27 ºC in the dark. (7 – 12) were taken using normal compound microscope, different shapes of spores of isolated fungi. Bar 10 µm in all pictures.
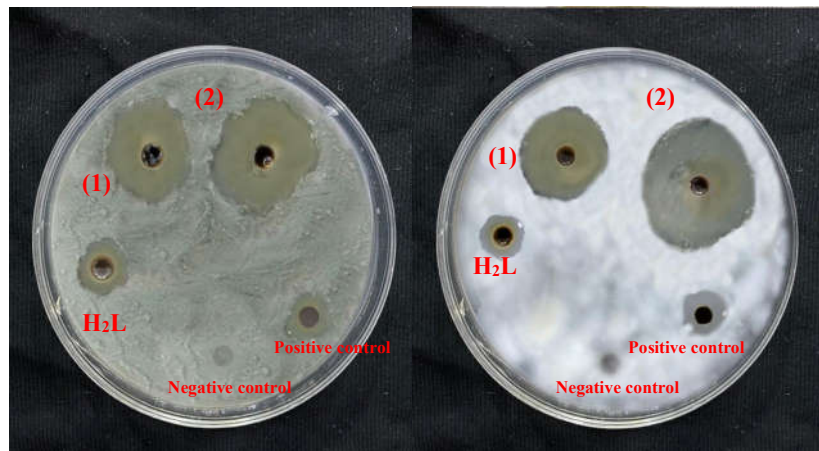
Figure 6b. Inhibition of mycelial growth of isolated fungi on PDA at 26 °C for 6 days in the dark.

Alternaria Alternata, *Aspergillus niger*, *Cladosporium cladiosporioides*, *Penicillium sp*, *Paecilomyces sp* and *Fusarium sp* were isolated from wall paper (Figure 6a). The present study reported that *Fusarium* sp was the most frequent fungus and represented 48.74% of the total count, followed by *A. niger* that was recovered from 4 samples matching 43.62% of total count fungal isolates. *Cladosporium cladiosporioides* represented 41.47% of the total count, while *Penicillium spp* gave 33.59% of the total count. *Paecilomyces sp* was found in 20.76% of the total fungi, whereas *Alternaria* species had the lowest value obtained sharing 14.01%.

MIC (minimum inhibitory concentration) and MFC (minimum fungicide concentration) values of different concentrations of 0.005, 0.01, 0.02, 0.04, 0.05, 0.1, 0.2, 0.3, 0.4 and 0.5 mg/mL were recorded by the standard serial dilution method against tested microbes using the broth macro-dilution technique. No turbidity was observed at 0.01 mg/mL in complex (**2**) of all isolated fungi, but in complex (**1**) the MIC concentrations was 0.04 and 0.05 mg/mL. Thus, it could be concluded that complex (**2**) has very good antibacterial activity by minimum inhibitory concentration (MIC) method.

Here is the proven order of outcomes: The hierarchy goes as follows: complex (**2**) > complex (**1**) > **H₂L**. The significant antibacterial activity of complex (**2**) may result from nanoparticle binding to microbial surfaces, cell membrane rupture, modification of the respiration chain and other permeability-dependent activities, and finally destruction of microbial [34]. In this study, complex (**2**) showed the highest biological activity of all the treatments utilized, totally preventing the growth of the evaluated species, as determined by measuring their ability to suppress the mycelial growth of each of the tested organisms. The biological activity of complex (**2**) against all fungal isolates increased with increasing concentration, as demonstrated in (Figure 6b).

The antifungal properties of the treated wallpaper were evaluated using every isolated fungus. As shown from the data, treated paper had fewer fungal colonies than the control group. The presence of treated wallpaper may alter fungal growth and nutrient absorption, and the results showed that complex (**2**) demonstrated antifungal capabilities. The bacteriostasis rate after one month was 100%, after 6 months was 85% and after one year was 68%. These results conclusively demonstrate the treated wallpaper's superior antifungal effect. The wallpaper that caved in with complex (**2**) is a good bio-resistance paper.

CONCLUSION

The Schiff base ligand (S,E)-2-((2-hydroxy-3-methoxybenzylidene)amino)-3-(1H-imidazol-4-yl)propanoic acid has been synthesized with its Ce(III) and Fe(III) complexes both in bulk and nano size. The complexes were described via various physicochemical approaches such as FT-IR, ^{1}H NMR, ^{13}C NMR, TGA, and SEM. The synthesized ligand and its metal complexes were investigated as antifungal agents. It was found from the results that the cerium nano complex shows a potent antifungal activity for indoor uses as wallpapers.

REFERENCES

1. Aleksic, B.; Draghi, M.; Ritoux, S.; Bailly, S.; Lacroix, M.; Oswald, I.P.; Bailly, J.-D.; Robine, E. Aerosolization of mycotoxins after growth of toxinogenic fungi on wallpaper. *Appl. Environ. Microbiol.* **2017**, 83, e01001-17.
2. Shirakawa, M.A.; Gaylarde, C.C.; Gaylarde, P.M.; John, V.; Gambale, W. Fungal colonization and succession on newly painted buildings and the effect of biocide. *FEMS Microbiol. Ecol.* **2002**, 39, 165-173.
3. Mendell, M.J.; Mirer, A.G.; Cheung, K.; Tong, M.; Douwes, J. Respiratory and allergic health effects of dampness, mold, and dampness-related agents: A review of the epidemiologic evidence. *Environ. Health Perspect.* **2011**, 119, 748-756.
4. Quansah, R.; Jaakkola, M.S.; Hugg, T.T.; Heikkinen, S.A.M.; Jaakkola, J.J. Residential dampness and molds and the risk of developing asthma: A systematic review and meta-analysis. *PLoS One* **2012**, 7, e47526.
5. Moustafa, S.M.N.; Taha, R.H.; Mycogenic nano-complex for plant growth promotion and bio-control of *Pythium aphanidermatum*. *Plants* **2021**, 10, 1858.
6. Moustafa, S.M.N.; Taha, R.H.; Abdelzaher, H.M.A.; Elgebaly, H.A. Novel biosynthesis of Ag-nanocomplex for controlling *Verticillium wilt* disease of olive tree. *Arch. Phytopathol. Plant Prot.* **2022**, 55, 198-216.
7. Khatami, M.; Sharifi, I.; Nobre, M.A.; Zafarnia, N.; Aflatoonian, M.R. Waste-grass-mediated green synthesis of silver nanoparticles and evaluation of their anticancer, antifungal and antibacterial activity. *Green Chem. Lett. Rev.* **2018**, 11, 125-134.
8. Chaloupka, K.; Malam, Y.; Seifalian, A.M. Nanosilver as a new generation of nanoproduct in biomedical applications. *Trends Biotechnol.* **2010**, 28, 580-588.
9. Ogar, A.; Tylko, G.; Turnau, K. Antifungal properties of silver nanoparticles against indoor mould growth. *Sci. Total Environ.* **2015**, 521, 305-314.
10. Pitt, J.I.; Hocking, A.D. *Fungi and Food Spoilage*, Academic Press: CSIRO Division of Food Research, Sidney, Australia; **1985**.
11. Klich, M.A. Biogeography of *Aspergillus species* in soil and litter. *Mycologia* **2002**, 94, 21-27.
12. Mohapatra, R.K.; El-ajaily, M.M.; Alassbaly, F.S.; Sarangi, A.K.; Das, D.A.; Maihub, A.S.; Ben-Gweirif, F.; Mahal, A.; Suleiman, M.; Perekhoda, L.; Azam, M.; Al-Noor, T.H. DFT, anticancer, antioxidant and molecular docking investigations of some ternary Ni(II) complexes with 2-[(E)-[4-(dimethylamino)phenyl]methyleneamino]phenol. *Chem. Pap.* **2021**, 75, 1005-1019.
13. Al-Noor, T.H.; Mohapatra, R.K.; Azam, M.L.; Karim, K.A.; Mohapatra, P.K.; Ibrahim, A. A.; Parhi, P.K.; Dash, G.C.; El-ajaily, M.M.; Al-Resayes, S.I.; Raval, M.K.; Pintilie, L. Mixed-ligand complexes of ampicillin derived Schiff base ligand and Nicotinamide: Synthesis, physico-chemical studies, DFT calculation, antibacterial study and molecular docking analysis. *J. Mol. Struct.* **2021**, 1229, 129832.

14. Rhoda, O.; Oyewole A.K.; Oyebamiji B.S. Theoretical calculations of molecular descriptors for anticancer activities of 1,2,3-triazole-pyrimidine derivatives against gastric cancer cell line (MGC-803): DFT, QSAR and docking approaches. Heliyon. 2020, 6, e03926.

15. Hussein, Y.; El-Fakharany, E.M.; Kamoun, E.A.; Loutfy, S.A.; Amin, R.; Taha, T.H.; Amer, M. Electrospun PVA/hyaluronic acid/L-arginine nanofibers for wound healing applications: Nanofibers optimization and in vitro evaluation. *Int. J. Biol. Macromol.* **2020**, 164, 667-676.

16. Taha, R.H.; El-Shafiey, Z.A.; Salman, A.A.; Mansour, M.M. A study of a newly synthesized ligand and its metal complexes in bulk and nano size and metal uptake efficiency. *Appl. Organomet Chem.* **2020**, 34, e5792.

17. Fard, M.J.S.; Esmaielzadeh, S.; Parsam, S.; Nejad, A.R. Hydrothermal synthesis of copper(II) and nickel(II) nano-complexes with asymmetric tetradentate Schiff base ligand; A new precursor for preparation of copper(II) and nickel(II) oxide nano-particles. *Nanachem. Res.* **2018**, 3, 197-204.

18. Sempere, F.; Santamarina, M.P.; Microscopic and macroscopic study of the interaction between Alternaria alternata (Fr.) Keissler and Nigrospora oryzae (Berk. & Broome) Petch. *Ann. Microbiol.* **2006**, 56, 101-107.

19. Monmi, P.; Thuong, T.T.N.; Hyang, B.L. Seven undescribed *Aspergillus* species from different niches in Korea. *Mycobiology*, **2022**, 50, 189-202.

20. Meskini, M. Esmaeili, D.; Ghorbani, M.; Alizadehgan, M.G. Comparison of Micro-dilution and Macro-dilution Methods for MIC Determination of Plant Extracts. Conference: The 5th national & the 1th International Congress on Novel & Innovative Laboratory Technologies October **2017**.

21. Taha, R.H.; Moustafa, Sh.M.N.; Hamza, H.T.; Bio-synthesis of Fe-nanocomplex using leaves *Ocimum basilicum L.* as a promising tool for tanning effluent treatment. *Biomass Convers. Biorefin.* **2023**, https://doi.org/10.1007/s13399-023-04139-3.

22. Rania, H.T.; Dalia, R.; Mohamed, Y. Nanofiber integrated nanocomplex as advanced technology for the treatment of pathogens-contaminated water at Jouf Region. *J. Polym. Environ.* **2023**, 31, 1-12.

23. Gade, M.; Comfort, N.; Re, D.B. Sex-specific neurotoxic effects of heavy metal pollutants: Epidemiological, experimental evidence and candidate mechanisms. *Environ. Res.* **2021**, 201, 111558.

24. Emam, S.M. Spectral characterization, thermal and biological activity studies of Schiff base complexes derived from 4,4′-Methylenedianiline, ethanol amine and benzil. *J. Mol. Struc.* **2017**, 1134, 444-457.

25. Rostamizadeh, S.; Daneshfar, Z.; Moghimi, H. Synthesis of sulfamethoxazole and sulfabenzamide metal complexes; evaluation of their antibacterial activity. *Eur. J. Med. Chem.* **2019**, 171, 364-371.

26. Angelusiu, M.V.; Barbuceanu, S.F.; Draghici, C.; Almajan, G.L. New Cu(II), Co(II), Ni(II) complexes with aroyl-hydrazone based ligand. Synthesis, spectroscopic characterization and in vitro antibacterial evaluation. *Eur. J. Med. Chem.* **2010**, 45, 2055-2062.

27. Habila, I.; Saoudi, M.; Berrah, F.; Benmerad, B.; Boudraa, M.; Merazig, H.; Bouacida, S. A new complex of zinc(II) with sulfamethoxazole ligand: Synthesis, crystal structure, Hirshfeld surface analysis, thermal properties, DFT calculations and antibacterial/antifungal activities. *J. Mol. Struc.* **2011**, 1244, 130903.

28. Alyar, S.; Özmen, Ü.Ö.; Adem, Ş.; Alyar, H.; Bilen, E.; Kaya, K. Synthesis, spectroscopic characterizations, carbonic anhydrase II inhibitory activity, anticancer activity and docking studies of new Schiff bases of sulfa drugs. *J. Mol. Struc.* **2021**, 1223, 128911.

29. Kavitha, A.; Easwaramoorthy, D.; Thangeeswari, T.; Parthipan, G.; Shanmugan, S.; Ansari, T. Synthesis and characterization of tritendate Schiff base rare earth nano metal complexes. *Mater. Today Proceed.* **2021**, 34, 453-459.

30. Mohamed, G.G.; Omar, M.M.; Hindy, A.M.M. Synthesis, characterization and biological activity of some transition metals with Schiff base derived from 2-thiophene carboxaldehyde and aminobenzoic acid. *Spectrochim. Acta A* **2005**, 62, 1140-1150.

31. Shah, R.K.; Abou-Melha, K.S.; Saad, F.A.; Yousef, T.; Al-Hazmi; G.A.; Elghalban, M.G.; El-Metwaly, N. Elaborated studies on nano-sized homo-binuclear Mn(II), Fe(III), Co(II), Ni(II), and Cu(II) complexes derived from N2O2 Schiff base, thermal, molecular modeling, drug-likeness, and spectral. *J. Therm. Anal. Calori.* **2016**, 123, 731-743.

32. Leung, C. H. ; Liu, L. J. ; Leung, K. H. ; Ma, D. L. Epigenetic modulation by inorganic metal complexes. Coord. Chem. Reviews. 2016, 319, 25-34.

33. Santoso, S.P.; Ismadji, S.; Angkawijaya, A.E.; Soetaredjo, F.E.; Go, A.W.; Ju, Y.H. Complexes of 2,6-dihydroxybenzoic acid with divalent metal ions: Synthesis, crystal structure, spectral studies, and biological activity enhancement. *J. Mol. Liq.* **2016**, 221, 617-623.

34. Chen, Y.C.; Yu, K.P.; Shao, W.C.; Tseng, C.H; Pan, W.C. Novel mold-resistant building materials impregnated with thermally reduced nano-silver. *Indoor Air* **2018**, 28, 276-286.